HHS Public Access

Author manuscript

Mol Cancer Ther. Author manuscript; available in PMC 2020 December 01.

Published in final edited form as:

Mol Cancer Ther. 2020 June ; 19(6): 1266–1278. doi:10.1158/1535-7163.MCT-19-0174.

Cabozantinib Reverses Renal Cell Carcinoma-Mediated Osteoblast Inhibition in Three-Dimensional Co-culture *In Vitro* and Reduces Bone Osteolysis *In Vivo*

Tianhong Pan[1], **Mariane Martinez**[2,3], **Kelsea M. Hubka**[2,4], **Jian H. Song**[5], **Song-Chang Lin**[6], **Guoyu Yu**[6], **Yu-Chen Lee**[6], **Gary E. Gallick**[5,**], **Shi-Ming Tu**[5], **Daniel A. Harrington**[2,3], **Mary C. Farach-Carson**[2,3,4], **Sue-Hwa Lin**[5,6,*], **Robert L. Satcher**[1,*]

[1]Department of Orthopedic Oncology, University of Texas, MD Anderson Cancer Center, Houston, TX, USA.

[2]Department of Diagnostic and Biomedical Sciences, University of Texas Health Science Center at Houston, School of Dentistry, Houston, TX, USA.

[3]Department of BioSciences, Rice University, Houston, TX, USA.

[4]Department of Bioengineering, Rice University, Houston, TX, USA.

[5]Department of Genitourinary Medical Oncology, University of Texas, MD Anderson Cancer Center, Houston, TX, USA.

[6]Department of Translational Molecular Pathology, University of Texas, MD Anderson Cancer Center, Houston, TX, USA.

Abstract

Renal cell carcinoma (RCC) bone metastases (RCCBM) are typically osteolytic. We previously showed that BIGH3 (beta Ig-h3/TGFbI), secreted by 786-O RCC, plays a role in osteolytic bone lesion in RCCBM through inhibition of osteoblast (OSB) differentiation. To study this interaction, we employed three-dimensional (3D) hydrogels to co-culture bone-derived 786-O RCC cells (Bo-786) with MC3T3-E1 pre-osteoblasts (OSB). Culturing pre-osteoblasts in the 3D hydrogels preserved their ability to differentiate into mature OSB; however, this process was decreased when pre-osteoblasts were co-cultured with Bo-786 cells. Knockdown of BIGH3 in Bo-786 cells recovered OSB differentiation. Further, treatment with bone morphogenetic protein 4 (BMP4), which stimulates osteoblast differentiation, or cabozantinib (CBZ), which inhibits VEGFR1 and MET tyrosine kinase activities, also increased OSB differentiation in the co-culture. CBZ also inhibited pre-osteoclast RAW264.7 cell differentiation. Using RCCBM mouse models, we showed that CBZ inhibited Bo-786 tumor growth in bone. CBZ treatment also increased bone volume and OSB number, and decreased osteoclast number and blood vessel density. When tested in SN12PM6 RCC cells that have been transduced to overexpress BIGH3, CBZ also inhibited

[*]**Co-Correspondence**: Sue-Hwa Lin, Department of Translational Molecular Pathology, Unit 89, The University of Texas MD Anderson Cancer Center, 1515 Holcombe Blvd., Houston, TX 77030. Phone: 713-794-1559; Fax: 713-834-6084; slin@mdanderson.org, Robert L. Satcher, Department of Orthopaedic Oncology, The University of Texas MD Anderson Cancer Center, 1515 Holcombe Blvd., Houston, TX 77030 Phone: 713-7942-4652; Fax: 713-792-8448; rlsatcher@mdanderson.org.
[**]Deceased

Conflict of interest disclosure: None

SN12PM6 tumor growth in bone. These observations suggest that enhancing OSB differentiation could be one of the therapeutic strategies for treating RCCBM that exhibit OSB inhibition characteristics, and that this 3D co-culture system is an effective tool for screening osteoanabolic agents for further *in vivo* studies.

Keywords

renal cell carcinoma; bone metastasis; 3D culture; co-culture; cabozantinib

Introduction

Renal cell carcinoma (RCC) accounts for 3% of all cancers. The most common metastasis for RCC occurs in lung, followed by bone lesions in 20–35% of patients with RCC (1). Renal cell carcinoma bone metastases (RCCBM) typically exhibits osteolytic lesions. Osteolytic lesions have a significant impact on patient mobility and survival and remain a major challenge in the treatment of RCC (2). Osteolytic bone metastasis is likely induced by tumor-bone interactions that cause imbalance in bone homeostasis, resulting in uncontrolled bone resorption (3–5). Although factors that promote bone destruction via osteoclast activation have been shown to be involved in RCC-induced osteolytic bone lesions, osteoclast-targeted agents do not appear to affect survival. Thus far, data on the role of osteoclast-targeted therapy in RCCBM are limited (6). We recently reported that BIGH3, a transforming growth factor-beta-induced protein ig-h3 (TGFBI) secreted by 786-O RCC, suppresses osteoblast (OSB) differentiation and reduces the healing of osteolytic lesions in RCCBM (7). In addition to BIGH3, we also detected IL-6 in 786-O conditioned medium (CM) (7). Both the BIGH3 and IL-6 have been reported to inhibit osteoblast differentiation (8,9). Thus, multiple factors, including BIGH3, contribute to the osteolytic bone lesions in 786-O RCC. According to this observation, stimulating OSB differentiation may be an effective strategy to improve the therapeutic outcome of anti-RCCBM treatment. We previously found that cabozantinib (CBZ) stimulates osteoblast differentiation (10). In addition, CBZ has been approved for RCC treatment (11,12). Thus, we examined whether CBZ can be used for treatment of RCC bone metastasis. BMP4 is known to stimulate osteoblast differentiation (13). We used BMP4 in this study as a positive control in our *in vitro* study. We propose that agents that have been shown to enhance OSB differentiation, e.g. cabozantinib (CBZ), and bone formation, e.g. BMP4 could limit osteolytic bone lesion from BIGH3.

To screen agents that can enhance OSB differentiation, we first established an *in vitro* model that mimics *in vivo* interactions between RCC cells and OSBs. We and others have shown that three-dimensional (3D) culture mimics the bone microenvironment more accurately than traditional 2D culture (14–17), and that bone-derived human 786-O RCC cells (Bo-786) grew as multicellular spheroids in 3D culture (18). In this study, we employed a 3D co-culture system that allowed us to interrogate the inhibitory effects of BIGH3 from RCC cells on OSB differentiation. We also used the 3D co-culture system to examine the effect of CBZ and BMP4 on overcoming the inhibitory effects of BIGH3 on OSB

differentiation. The results from these *in vitro* studies led us to perform *in vivo* studies to examine the effects of CBZ on RCCBM.

Materials and Methods

Cell culture

Human 786-O RCC cells, murine pre-osteoblast cells (MC3T3-E1 clone 4) and the mouse pre-osteoclast RAW 264.7 cells were purchased from American Type Culture Collection (ATCC, Manassas, CA). SN12PM6 RCC cells were purchased from MD Anderson Cancer Center Characterized Cell Line Core Facility. Bone-derived 786-O (Bo-786) RCC cells were generated from the human 786-O cell line through *in vivo* selection as described previously (19,20). Bo-786 cells with BMP4 overexpression (Bo-786/BMP4), were generated by infecting Bo-786 cells with retroviruses containing human BMP4 cDNA in a bicistronic retroviral vector (pBMN-BMP4-I-neo) as reported previously (20,21). Bo-786 cells expressing pBMN-I-neo vector were used as control (Bo-786/Vector). To express luciferase in SN12PM6 RCC cells for *in vivo* study, human SN12PM6 RCC cells were transduced with a lentiviral vector containing cDNA encoding for luciferase (Luc) and red fluorescent protein (RFP) genes (pCDH-EF1-Luc-RFP plasmid). Lentiviral particles, generated in HEK293 cells 48 hours after pCDH-EF1-Luc-RFP plasmid transfection using Lipofectamine 2000 (Thermo Fisher Scientific), were used for infecting SN12PM6 RCC cells. The infected cells were selected for high RFP level by fluorescence-activated cell sorting (FACS) and termed SN12PM6/LR cells (SN12PM6/Luc-RFP). SN12PM6/LR cells with BIGH3 overexpression (SN12PM6/LR/BG) and its vector control (SN12PM6/LR/Vector) were generated by infecting SN12PM6/LR cells with retroviruses containing human BIGH3 cDNA in a bicistronic retroviral vector (pBMN-BIGH3-I-neo) as described above. Bo-786 cells with BIGH3 knockdown (Bo-786/BG#3shRNA and Bo-786/BG#4shRNA) and control cells (Bo-786/NS shRNA) were generated as reported previously (7). Bo-786 cells and derived cells were cultured in RPMI-1640 medium (Invitrogen, Carlsbad, CA). MC3T3-E1 cells were cultured in Alpha-Minimum Essential Medium (α-MEM, Life Technologies, Grand Island, NY). SN12PM6 cells and derived cells, RAW264.7 cells were cultured in Dulbecco's Modified Eagle Medium (DMEM, Invitrogen, Carlsbad, CA). All media contained 10% (v/v) fetal bovine serum (FBS), 100 U/mL penicillin and 100 mg/mL streptomycin (Invitrogen Corporation, Carlsbad, CA, USA). In co-culture studies, a 1:1 (v/v) mixture of RPMI-1640 and α-MEM medium supplemented with 10% (v/v) FBS was used for both control monoculture and co-culture. The osteogenic differentiation medium (ODM) used in this study refers to a 1: 1 (v/v) mixture of RPMI-1640 and alpha-MEM medium containing β-glycerol phosphate (5 mM, Sigma-Aldrich Co., St Louis, MO) and L-ascorbic acid (100 μg/mL, Sigma-Aldrich Co., St Louis, MO). All cells were incubated at 37°C in a humidified atmosphere of 5% CO_2 and 95% air. The passages of cells used in the experiments were between passages 6 to passages 20 and were routinely checked for the absence of mycoplasma contamination using the MycoAlert™ PLUS Mycoplasma Detection Kit (Lonza, Rockland, ME) according to manufacturer's instructions. Cabozantinib (CBZ), a small-molecule tyrosine kinase inhibitor that potently targets MET, VEGFR2, and several other receptor tyrosine kinases (22), was provided by Exelixis (Alameda, CA). CBZ was dissolved in DMSO for *in vitro* study and was formulated in

hydrochloric acid (HCl)-added sterile water (1 mL water + 10 μL 1N of HCl) for administration via oral gavage. Recombinant Human BMP-4 protein was purchased from R&D Systems, Inc. (Minneapolis, MN).

Cell line authentication

All the human cell lines were authenticated by STR analysis at MD Anderson Cancer Center Characterized Cell Line Core Facility

Cell encapsulation in HA hydrogel

The 3D hydrogel was constructed by mixing thiol-modified hyaluronic acid (HA-SH, 10 mg/mL in DG H_2O, Glycosil, BioTime Inc., Alameda, CA) with acrylate-PEG-GRGDS (73.7 mg/mL in PBS) and acrylate-PEG-PQ-PEG acrylate (37.0 mg/mL in PBS) at a volume ratio of 4:1:1 as described previously (23). Each puck in the custom-made mold contains 42 μL of 3D hydrogel. The number of OSB or Bo-786 for each puck was 100,000 cells. For monoculture, cells encapsulated in 21 μL of 3D gel were pipetted onto a layer of acellular hydrogel (21 μL) pre-loaded in the custom-made mold. For co-culture, Bo-786 (100,000 cells) and OSB (100,000 cells) were mixed and encapsulated in 42 μL of 3D gel, followed by pipetting into custom-made molds. Thus, each type of cell was seeded at a final density of 2.4×10^6 cells/mL. After incubation at 37°C for 45 minutes, the hydrogel pucks were immersed in cell culture medium and were incubated at 37°C overnight. The hydrogel pucks were then removed from molds and transferred into a 48-well plate, and media were exchanged every 2 days.

Sample preparation for DNA, calcium content, and alkaline phosphatase (ALP) activity

At indicated time point, cell-hydrogel pucks were washed with calcium-free PBS followed by adding ddH_2O (50 μL/puck). Hydrogel pucks were then underwent three freeze/thaw cycles followed by sonication (Bransonic Ultrasonic Cleaner, 5510R-DTH, Branson Ultrasonics Corporation, Danbury, CT) at room temperature for 30 minutes. Samples were then centrifuged (10,000 rpm, 10 minutes, 4°C) and the supernatant was collected for measuring ALP activity and DNA content. The gel fragment fractions were washed with calcium-free PBS to remove soluble calcium and was saved for calcium assay (see below). Hydrogel pucks without cells were used as controls.

DNA content was determined by assaying 20 × diluted aliquots of supernatant using PicoGreen Assay Kit (Molecular Probes, Eugene, OR) following the manufacturer's instructions. The fluorescence was read on a microplate reader (FLUOstar Omega multi-mode microplate reader, BMG LABTECH Inc.Cary, NC, USA) using an excitation wavelength of 480 nm and an emission wavelength of 520 nm.

ALP activity was determined using phosphatase substrate p-nitrophenol phosphate (PNPP). Briefly, 50 μL of the supernatant was added into the wells of 96-well microplate (Corning™ Costar™ Flat Bottom Cell Culture Microplates, Cat# 3595, Fisher Scientific Co. L.L.C.) containing 150 μL of PNPP solution (1 mg/mL in diethanolamine substrate buffer; Thermo Scientific, Rockford, IL). The plate was kept in dark for 30 minutes and the ALP enzyme

activity was measured with a microplate reader as indicated above at an absorbance wavelength of 405 nm.

The extracellular matrix (ECM) calcium deposit was determined using calcium Arsenazo III reagent (Pointe Scientific, Inc., Canton, MI) that measures the amount of blue-purple-colored calcium-Arsenazo^{2+} complex formed when Arsenazo III binds to free calcium in an acidic solution. Briefly, 1 M acetic acid (sigma) (42 μL/puck) was added to the resulting gel fragment fraction as indicated above. After rotating overnight, samples were centrifuged at 10,000 rpm for 15 minutes. The resulting supernatant (15 μL) was added to 96-well plate containing150 μL of Arsenazo III reagent. The absorbance was read on a microplate reader at 650 nm. Hydrogel pucks without cells were processed in parallel and used as blank controls.

For ALP staining of OSB differentiated in 2D culture, BCIP/NBT (SigmaFast BCIP-NBT; Cat# B5655, Sigma-Aldrich, Inc. St. Louis, MO) was used according to manufacturer's instructions.

Osteoclast differentiation and Tartrate-Resistant Acid Phosphatase (TRAP) staining

RAW264.7 cells were stimulated with RANKL at 50 ng/ml in α-MEM culture media for 5 days with one fresh media change with RANKL on day 3. Differentiation of pre-osteoclast RAW264.7 cells was determined by TRAP staining using Acid Phosphatase, Leukocyte (TRAP) Kit (387A SIGMA) (Sigma). TRAP activity was measured using TRAP staining kit (KT-008, Kamiya Biomedical Company, Seattle, WA) according to manufacturer's instructions.

RNA extraction and real-time reverse transcription-polymerase chain reaction (RT-PCR)

Total RNA was isolated from hydrogel pucks using an RNeasy Mini Kit (Qiagen, Valencia, CA). Briefly, cell-hydrogel 3D construct pucks were washed with PBS and stored at −80°C until all samples were collected. On the day of assay, three or four of hydrogel pucks were suspended in 350 μL RLT buffer provided in RNeasy Mini Kit (Qiagen, Valencia, CA). Samples were blended using a Bullet Blender (24 Gold, Next Advance, Averill Park, NY) at 20 seconds low speed and 1 minute off cycle 3 times at 4°C. After blending, samples were centrifuged at 10,000 g for 10 minutes to remove the debris. The supernatant was used for total RNA preparation using RNeasy Mini Kit (Qiagen, Valencia, CA) according to the manufacturer's instructions, and cDNA was synthesized from 1 μg of total RNA by TaqMan Reverse Transcription Reagents (Life Technologies). Real-time PCR was carried out in the Multiplex Quantitative PCR System (STRATAGENE, Model Mx3000pTM) using SYBR Green PCR Super Mix (Applied Biosystems, CA) with the following PCR conditions: 40 cycles of 15 seconds denaturation at 95°C and 1 minute amplification at 60°C. All reactions were run in duplicates. The evaluation of relative differences of PCR results was calculated using the comparative cycle threshold (C_T) method with the housekeeping gene glyceraldehyde-3-phosphate dehydrogenase (GAPDH) for mouse or β-actin for human as internal control. The following primer sets were used: mouse ALP forward, 5′-AGCTCAACACCAATGTAGCC-3′ and reverse, 5′-GTAGCTGGCCCTTAAGGATT-3′; mouse osteocalcin (OSC) forward, 5′- GCTCTGTCTCTCTGACCTCA −3′ and reverse, 5′-

TGGACATGAAGGCTTTGTCA −3′; mouse GAPDH forward, 5′-GTGCAGTGCCAGCCTCGTCCCG-3′ and reverse, 5′-CTCCACTTTGCCACTGCAAATG-3′; human BIGH3 forward, 5′-ACTGAACCTGACCGTACACTGCAGCCTCCAGCCAAC −3′ and reverse, 5′-GTCTGCAAGTTCATCCCCTCTT −3′; human BMP4 forward, 5′-CAGCACTGGTCTTGAGTATCCTGA-3′ and reverse, 5′-CGTGTCCAGTAGTCGTGTGATGA −3′; human ALP forward, 5'-ACTGGTACTCAGACAACGAGAT-3' and reverse, 5'-ACGTCAATGTCCCTGATGTTATG-3'; human osteocalcin (OSC) forward, 5'-AGAGTCCAGCAAAGGTGCAG-3' and reverse, 5'-GGCTCCCAGCCATTGATACA-3'; human β-actin forward, 5′-GGGACCTGACTGACTACCTCA-3′ and reverse, 5′-CAGCTTCTCCTTAATGTCACG-3′.

Cell viability assay

Cell viability was determined using the LIVE/DEAD viability/cytotoxicity kit (Life Technologies) per the manufacturer's instructions. Specifically, cells in hydrogel were incubated with 2 μM calcein-AM and 4 μM ethidium homodimer at 37°C for 40 minutes before confocal imaging. Cell proliferation was determined using PrestoBlue cell viability assay kit (Thermo Fisher Scientific, Waltham, MA) or MTT (3-(4,5-dimethylthiazol-2-yl)-2,5-diphenyltetrazolium bromide, Sigma-Aldrich, St Louis, MO, USA) tetrazolium reduction assay (24).

Enzyme-linked immunosorbent assay (ELISA)

Osteocalcin protein level was determined using mouse Osteocalcin Enzyme Immunoassay Kit (BT-470; Biomedical Technologies). BMP4 protein level was determined using the RayBio Human BMP-4 ELISA kit (ELH-BMP4–1, RayBiotech, Inc., Norcross, GA).

Animal studies

All animal procedures were performed according to an approved protocol from MD Anderson's Animal Care and Use Committee, in strict accordance with the recommendations in the Guide for the Care and Use of Laboratory Animals of the National Institutes of Health. Bo-786, SN12PM6/Vector and SN12PM6/BG RCC cells grown to sub-confluence were harvested and resuspended in PBS to a final concentration of 20×10^7 cells/mL. Cells (5 μL of such cell suspension with a total of 1×10^6 cells) were injected directly into the distal end of the right femur of 5-week-old male SCID mice (Jackson Laboratory) using a 26-gauge needle. Two weeks after bone injection, CBZ was administrated via oral gavage at 20 mg/kg body weight in a volume of 100 μL, 2 times a day, 6 days a week for 18 to 39 days.

Bioluminescent imaging (BLI) and micro-computed tomographic evaluation (micro-CT)

The RCC tumor expansion in bone was monitored by measuring luciferase activity of RCC tumor cells by BLI using an IVIS 200 Imaging System (Xenogen). The photon signal intensity was quantified using Living-Image software version 2.5 (Caliper Life Science). At the conclusion of the study, mice were euthanized, and both the injected and contralateral

control femurs were collected and fixed in 10% paraformaldehyde for 48 hours, followed by washing with PBS and soaking in 70% ethanol. The femurs were then subjected to micro-CT analysis (MDACC Small Animal Imaging Facility) performed with an Enhanced Vision Systems hybrid specimen scanner (GE Medical Systems, London, ON, Canada) at a resolution of 90 μm. The images were reconstructed and bone mineral density (BMD) was analyzed using Microview (2.1.2) software provided by GE Healthcare.

Bone histomorphometry

Bone histomorphometry analysis on non-decalcified mouse femurs was performed by MDACC Bone Histomorphometry Core Laboratory. The regions located in the distal metaphysis of the femur starting 150 μm proximal to the growth plate and extending 1.3 mm towards the diaphysis were analyzed. The measurement area excluded the 150 μm area adjacent to the cortical bone. For each sample, measurements for OSBs and osteoclasts were performed on 2 separate 5 μm thick Toluidine Blue and TRAP stained sections, respectively. The sections were separated by a distance of 50 μm and the data pooled. Blood vessel quantification was performed on one Toluidine Blue stained 5μm thick bone section. Red blood cells stain distinctly and carry a partial phase contrast when stained with toluidine blue so quantification could be performed confidently. Blood vessel surface was traced, excluding OSB/osteoclast measurements, using Bioquant Osteo II software. Surface measurements and tissue volume were used to derive further values.

Statistical analysis

Data were expressed as mean ± standard deviation. Differences between paired data were tested using Student's *t* test (2-tailed, paired). Differences were considered significant at $P < 0.05$.

Results

Bo-786 RCC cells inhibit OSB differentiation in a 3D co-culture system

We previously reported that the HA-based 3D culture provides an improved platform for RCCBM studies compared with 2D systems (18) and that the hyaluronic acid (HA)-based 3D hydrogel containing GRGDS-peptide and MMP-labile "PQ" crosslinker is suitable for culturing pre-osteoblast MC3T3-E1 cells (23). In this study, we first determined OSB differentiation in osteogenic differentiation medium (ODM) in HA-based 3D hydrogels for 6 and 12 days. We found an elongated cell morphology characteristic of differentiated OSBs compared to culturing in regular medium as control (Fig. S1A). We then examined the expression of alkaline phosphatase (ALP), an early OSB marker, and osteocalcin (OSC), a late marker for osteogenic differentiation. Both ALP mRNA and ALP activity (Fig. S1B) and OSC mRNA and OSC protein levels (Fig. S1C) were significantly higher in ODM than in control medium at both day 6 and day12. Mineralization is one of the characteristics of mature OSBs. We conducted calcium assay and found that calcium deposit was also significantly higher in OSB cultured in ODM at day 6 and day 12 compared to controls (Fig. S1D). We selected day 6 as a time point for further study.

To examine RCC and bone microenvironment interaction, we co-encapsulated Bo-786 RCC cells with pre-osteoblast MC3T3-E1 (OSB) at a ratio of 1:1 in 3D hydrogels and cultured these hydrogels in ODM. The monoculture of OSB or Bo-786 cells were used as control. We showed that Bo-786 cells formed multicellular aggregates over 6 days (Fig. 1A), while OSBs remained single but exhibited a flattened elongated morphology (Fig. 1A). LIVE/DEAD viability/cytotoxicity assay indicated that cells in both mono- and co-cultures remained viable in the 3D hydrogels over 6 days (Fig. 1B). We further determined the effects of Bo-786 cells on OSB differentiation by co-culturing OSB with Bo-786 RCC cells in 3D hydrogels. It is possible that Bo-786 may express osteoblast markers as some metastatic cancer cells sometime are capable of osteomimetism (25). To examine such a possibility, we performed real-time RT-PCR using human-specific primers for ALP mRNA and OSC mRNA from Bo-786 cells. Human PC3 prostate cancer cells that express OSC were used as a positive control (26). We detected low mRNA levels of human ALP (about 7% of PC3) (Fig. S2A) and human OSC (about 20% of PC3) (Fig. S2B) in Bo-786 cells. However, the primers we used in qRT-PCR for detecting ALP and OSC mRNA in the co-culture are mouse-specific and did not generate detectable signals when used in Bo-786 cells (Fig. 1C). We found that the mouse ALP and OSC mRNAs as determined by quantitative real-time RT-PCR using mouse-specific primers were significantly lower in the co-cultures compared to those in OSB monocultures (Fig. 1C). In addition, ALP protein levels as determined by ALP activity assay (Fig. 1D), and OSC protein levels as determined by OSC ELISA (Fig. 1E), were also significantly lower in the co-cultures compared to those in OSB monocultures. Calcium assay also showed that calcium deposit was significantly less in the co-culture than in OSB monoculture (Fig. 1F). These results indicate that the *in vitro* 3D co-culture system may be useful for testing agents for their effects on OSB differentiation.

BIGH3 knockdown in Bo-786 cells increases OSB differentiation

We previously showed that BIGH3, secreted by 786-O RCC, exerts an inhibitory effect on OSB differentiation (7). To test the effects of BIGH3 on OSB differentiation in the 3D co-culture system, we knocked down BIGH3 in Bo-786 cells (Bo-786/BG#3sh, Bo-786/BG#4sh). The non-silencing cells (Bo-786/NS) were used as control. We observed a significant decrease of BIGH3 mRNAs in Bo-786/BG#3sh and Bo-786/BG#4sh cells compared to Bo-786/NS cells (Fig. 2A). We co-cultured these cells with pre-OSBs in ODM. ALP mRNA as well as ALP activity were significantly increased when OSBs were co-cultured with Bo-786/BG#3sh or Bo-786/BG#4sh, as compared to those co-cultured with Bo-786/NS cells (Fig. 2B). Similar increases were observed in OSC mRNA and OSC protein levels (Fig. 2C) and in calcium deposit levels (Fig. 2D) in Bo-786/BG#3sh and Bo-786/BG#4sh cells versus control cells. These results showed that BIGH3 has inhibitory effects on OSB differentiation in the 3D co-culture system, and further support the utility of this system for screening agents that may affect OSB differentiation.

BMP4 reverses Bo-786-mediated inhibition of OSB differentiation in 3D co-culture

Bone morphogenetic protein 4 (BMP4) is a protein factor that induces bone formation. Our previous study found that BMP4 treatment at 100 ng/mL increased OSB differentiation (13). To examine whether BMP4 can overcome OSB inhibition by Bo-786 cells, we treated OSBs in monoculture or in co-culture with Bo-786 cells with recombinant BMP4 at the

concentration of 100 ng/mL. BMP4 was added with each change of medium every other day. Treatment with recombinant BMP4 increased OSB differentiation markers including ALP (Fig. 3A, left) and OSC (Fig. 3A, middle) at both mRNA and protein levels. Similarly, calcium deposits were also increased with BMP4 treatment (Fig. 3A, right). Next, we overexpressed human BMP4 in Bo-786 cells (Bo-786/BMP4). The BMP4 mRNA and protein levels in Bo-786/BMP4 cells were significantly higher than those in vector control cells (Bo-786/Vector) as determined by real-time RT-PCR and ELISA (Fig. 3B). When OSBs were grown in 2D and cultured in ODM for 14 days, treatment with Bo-786/Vector conditioned medium (CM) caused a significant decreased in ALP protein level as determined by ALP staining and ALP activity assay (Fig. 3C). The inhibition was attenuated when OSBs were treated with Bo-786/BMP4 CM (Fig. 3C). On the other hand, co-culture of OSBs with Bo-786/BMP4 in 3D resulted in higher levels of ALP (Fig. 3D, left), OSC (Fig. 3D, middle), and calcium deposit (Fig. 3D, right) compared to those co-cultured with Bo-786/Vector cells. These results demonstrated that BMP4 can overcome Bo-786-mediated inhibition of OSB differentiation in the 3D co-culture system.

Cabozantinib (CBZ) enhances OSB differentiation

Cabozantinib (CBZ) is a small molecular tyrosine kinase inhibitor that has been recently approved for treating patients with advanced stage RCC (11,27). CBZ has antitumor effects *via* inhibition of VEGFR2 and MET (27,28). We and others also showed that CBZ is active in the bone microenvironment as it enhances OSB differentiation (10,29,30). We treated OSBs with CBZ either in 3D monoculture (Fig. 4A) or 3D co-culture with Bo-786 RCC cells (Fig. 4B). We found that CBZ treatment enhanced OSB differentiation as demonstrated by the increases in mRNA and protein levels of ALP and OSC, as well as in calcium deposits. Interestingly, Bo-786 cell viability was not affected by CBZ treatment for up to 6 days in 3D culture (Fig. 4C). We also did not observe changes of cell viability in OSB monoculture (Fig. 4D) or OSB-Bo-786 co-culture (Fig. 4E). These results are anticipated as the antitumor effect of CBZ *in vivo* is *via* inhibition of VEGFR2 on endothelial cells (27,28). These results indicate that CBZ can partially reverse Bo-786-mediated inhibition of OSB differentiation.

To examine the effect of CBZ on osteoclasts, pre-osteoclast RAW264.7 cells were induced to differentiate into osteoclasts by RANKL and treated with or without CBZ for 5 days. TRAP staining showed that RANKL caused RAW264.7 cells to form TRAP positive multinuclear cells. Control cells without RANKL treatment were negative with TRAP staining (Fig. 4F). TRAP activity was 4.5-fold higher in RANKL-treated cells than that in negative control cells (Fig. 4F). Treatment with 100 nM or 500 nM CBZ led to a decrease in TRAP activity by 26% and 50%, respectively (Fig. 4F). These results indicate that CBZ inhibits the differentiation of pre-osteoclast RAW264.7 to osteoclasts. We also treated pre-osteoclast RAW264.7 cells with Bo-786 CM and found that Bo-786 CM increased the formation of TRAP-positive multinuclear cells (Fig. 4G) with an increase in TRAP activity by 1.25-fold compared to negative control (Fig. 4G). These observations suggest that Bo-786 CM contains factors that stimulate osteoclast activity. Importantly, we found that CBZ treatment reduced Bo-786 CM-mediated increase in TRAP activity (Fig. 4G).

Effects of CBZ on Bo-786 RCC growth in bone and on the bone microenvironment *in vivo*

Since Bo-786 RCC-mediated inhibition of OSB differentiation is one of the mechanisms that lead to bone osteolysis (7), enhancing OSB differentiation might be a promising therapeutic strategy for treating/preventing osteolytic RCCBM. We thus further tested CBZ effects on Bo-786 RCC tumor growth in bone *in vivo*. Because we focused on the treatment of tumor growth in bone in this study, not the prevention of bone metastasis, we used intra-femoral injection of mice with Bo-786 RCC cells as an *in vivo* model (7). Due to the heterogeneity in the sizes of tumors in bone, we ranked tumor sizes by their bioluminescence intensity 14 days after tumor inoculation, and tumors with similar sizes were paired for vehicle (Bo-786/Con) or CBZ (Bo-786/CBZ) treatment. After CBZ treatment for 18 days, 5 of the control tumors reached the sizes that may have impending bone break due to strong osteolytic bone lesions from Bo-786 cells. Thus, these 5 pairs were terminated early. CBZ treatment for the rest of the pairs with smaller tumor sizes were continued for an additional 21 days. As shown in Fig. 5A, the BLI signal was significantly increased over 18 days in control mice without CBZ treatment (Bo-786/Con) as compared to day 0 (Fig. 5A, n = 5), indicating continued growth of Bo-786 RCC in bone. However, the increase in BLI signal was less in CBZ-treated mice (Bo-786/CBZ) than that in vehicle control mice (Bo-786/Con) (Fig. 5A), indicating that CBZ treatment inhibited tumor growth in bone. Micro-CT showed that Bo-786 (Bo-786/Con) growth in bone induced osteolysis (Fig. 5B). In CBZ-treated mice (Bo-786/CBZ), osteolysis was reduced relative to untreated controls (Fig. 5B). The CBZ-treated mice showed a trend of increased bone mineral density (BMD) and bone volume fraction (BVF, BV/TV); however, this trend did not reach statistical significance (Fig. 5B, right). Bone histomorphometry analysis detected a trend of increased number of OSBs per osteoid perimeter (N. Ob/O.Pm), increased bone volume (BV/TV%), and a significant increase of trabecular thickness (Tb. Th) in the CBZ-treated group compared to the control group (Fig. 5C), indicating that CBZ has an effect on OSB differentiation *in vivo*. Because CBZ inhibits VEGFR2, we also determined the effects of CBZ on angiogenesis in the *in vivo* model. We quantified the blood vessel volume (BVV) and blood vessel surface (BVS) on Toluidine Blue stained bone sections. We found that there was a significant decrease in blood vessel density (BVS/BVV) in CBZ-treated group compared to the untreated group (Fig. 5D), indicating an inhibitory effect of CBZ on angiogenesis. To determine the CBZ effects on osteoclasts in the *in vivo* model, we quantified osteoclasts on TRAP stained bone sections (Fig. 5E). Our results showed that there was a significant reduction in TRAP staining in the CBZ-treated tumors compared to untreated tumors (Fig. 5E). The number of osteoclasts counted in the measurement area (Oc Number), the number of osteoclasts per erosion perimeter (N. Oc/E.Pm), and the number of osteoclasts per bone perimeter (N. Oc/B. Pm) were all significantly lower in CBZ-treated group than those in the untreated group (Fig. 5E). These results indicate that CBZ has an inhibitory effect on osteoclast differentiation *in vivo*. The growth of RCC in bone in the remaining 10 mice in each group were continuously monitored by BLI for a total of 39 days after initiating CBZ treatment. Similar to those observed with large tumors, the BLI in the control untreated group were increased over 39 days (Bo-786/Con, Fig. 5F, n = 10). The BLI in CBZ-treated group was significantly lower (Bo-786/CBZ, n=10) than that in control mice (Fig. 5F). Together, these results suggest that CBZ has effects on both Bo-786 RCC tumor growth in bone and the bone microenvironment.

Effects of CBZ on SN12PM6 RCC growth in bone

To address whether our observation in Bo-786 cells also applies to other RCC cells, we examined the effect of CBZ on human SN12PM6 RCC cells (31). Our previous study showed that SN12PM6 cells express very low levels of BIGH3 (7). Thus, we overexpressed BIGH3 in SN12PM6 cells. Real-time RT-PCR results showed that the BIGH3 mRNA levels were significantly higher in SN12PM6/BG cells than in SN12PM6/Vector control cells (Fig. 6A). MTT assay showed that there was no significant difference in cell proliferation rate between these two cell lines (Fig. 6B). To determine the effects of CBZ on SN12PM6 RCC cell proliferation *in vitro*, we treated these two cell lines with CBZ at concentrations of 0, 50 nM and 100 nM for over 5 days. Our results showed that CBZ treatment did not cause inhibition of cell growth in either cell lines (Fig. 6C).

To determine whether CBZ can inhibit SN12PM6 RCC growth in bone, we injected mice with SN12PM6/Vector or SN12PM6/BG RCC cells intra-femorally. Tumors were allowed to grow in bone for two weeks followed by CBZ treatment for an additional 21 days. We found that the BLI signals were increased over the time period of 21 days in both SN12PM6/Vector (SN12PM6/Vector-Con) (Fig. 6D, n = 7) and SN12PM6/BG (SN12PM6/BG-Con)-injected femurs (Fig. 6E, n = 7). CBZ treatment decreased BLI signals in both SN12PM6/vector-injected mice (Fig. 6D, n = 7) and SN12PM6/BG-injected mice (Fig. 6E, n = 7). These results indicate that CBZ inhibits the growth of human SN12PM6/Vector and SN12PM6/BG RCC cells in bone. Because the luciferase levels in SN12PM6/Vector and SN12PM6/BG cells are different, whether there is difference in the growth rate between these two cell lines *in vivo* is not clear.

Bone histomorphometry analysis on femurs bearing SN12PM6/BG RCC was performed. We detected a trend of increased number of OSBs per osteoid perimeter (N. Ob/O.Pm), increased bone volume (BV/TV%), and a significant increase of trabecular thickness (Tb. Th) in CBZ-treated group compared to the control group (Fig. 6F). CBZ treatment caused a significant decrease in blood vessel density (BVS/BVV) as compared to the controls (Fig. 6G). CBZ treatment also caused a significant decrease in the number of osteoclasts counted in the measurement area (Oc Number), as well as the number of osteoclasts per bone perimeter (N. Oc/B. Pm), and showed a trend of decrease in the number of osteoclasts per erosion perimeter (N. Oc/E.Pm) as compared to control (Fig. 6H). Taken together, CBZ treatment promotes OSB differentiation and inhibits angiogenesis and osteoclast differentiation *in vivo*.

Discussion

We used *in vitro* 3D hydrogel co-culture of Bo-786 RCC cells with pre-OSB MC3T3-E1 cells to mimic the RCC-OSB interactions in osteolytic RCC bone metastasis. In this 3D culture system, OSB differentiation was inhibited when co-cultured with Bo-786 RCC. We also showed that BMP4 and CBZ, which enhance OSB differentiation, reversed the OSB inhibition induced by co-culturing with RCC cells. Moreover, we showed that CBZ is effective in inhibiting RCC growth in bone and also reduces the extent of osteolytic bone lesions *in vivo*. Our studies thus provide pre-clinical evidence for the application of CBZ in the treatment of RCCBM. CBZ has been approved for treatment of advanced RCC. Our

studies suggest that CBZ also have efficacy against RCCBM. We propose that agents that enhance OSB differentiation may be useful as a therapeutic strategy for treating RCCBM that is resistant to antiresorptive agents. The 3D co-culture system described in this study could be used for evaluating the potential of bone anabolic agents alone or in combination with anti-tumor agents for further *in vivo* studies.

RCCBM is almost exclusively osteolytic. The bone microenvironment is crucial to the pathogenesis of osteolysis associated with RCC. A “vicious cycle” produced by a positive feedback interaction between tumor and resident bone cells leads to disruption in physiological homeostasis, causing pathological bone resorption. Resistance to anti-resorptive agents suggests that bone formation mechanisms are also pathologically impacted. We recently reported that BIGH3, a paracrine factor secreted by RCC cells, is involved in osteolytic RCCBM via inhibition of OSB differentiation (7). BIGH3, also known as TGFBI (transforming growth factor beta induced protein), is a secreted 68-kD, 683 amino acid protein, not previously linked to osteolysis. Our studies showed that BIGH3 secreted by RCC cells potentially promotes osteolysis by inhibiting OSB differentiation (7). Whether this is a significant contributor to pathologic osteolysis in RCC has not been previously evaluated. In the current study, we confirmed a direct inhibition of OSB differentiation by closely apposed RCC cells (Bo-786) that secrete high levels of BIGH3. BIGH3 is an extracellular matrix (ECM) protein with motifs interacting with the alpha3beta1, alphavbeta5, and alphavbeta3 integrins. Although inhibition of integrins is one way to overcome BIGH3-mediated osteoblast inhibition, we did not use such an approach because of the possible involvement of multiple integrins and the presence of other osteoblast inhibition factors, e.g. IL6 (9). As a proof-of-concept, we evaluated whether RCC-induced OSB inhibition could be reversed using osteoanabolic agents. The bone anabolic agent BMP4 (32), which stimulates osteogenesis through Smad1/5 signal transduction (33), reversed the RCC-mediated inhibition of OSB differentiation in the 3D co-culture system, suggesting a novel strategy of using osteoanabolic agents for treating pathologic osteolysis that is resistant to anti-resorptive agents.

CBZ is a small molecule that targets MET, AXL, and VEGF receptors and has recently been approved for treating advanced RCC patients (11,12). MET is overexpressed in bone metastases specimens from patients with RCCBM (34). Recent clinical data demonstrate that CBZ improves progression-free survival in patients with advanced RCC (35–37). In a subgroup analysis, patients with RCCBM benefited from CBZ compared with the mTOR kinase inhibitor, everolimus (38). Evidence suggests that CBZ may enhance the OSB reparative response (39) and therefore provides a strategy to overcome resistance to anti-osteoclast treatment. The observed reduction of bone osteolytic lesions by CBZ in our mouse model of RCCBM *in vivo* could be explained by the dual functions of CBZ on inhibiting tumor angiogenesis and on normalization of the bone microenvironment. We did not observe significant decreases in cell viability from treating Bo-786 cells with CBZ *in vitro*, suggesting that targeting MET alone on RCC cells is not sufficient for tumoricidal efficacy. This observation is consistent with the previous report that CBZ has no effect on PCa cell proliferation *in vitro* (40). Rather, the tumoricidal efficacy of CBZ in vivo is also dependent on its anti-angiogenesis activity. We also showed that CBZ affects both OSB and osteoclasts *in vivo* resulting in the reduced osteolytic bone lesions from RCC. The

enhancement of OSB differentiation by CBZ is consistent with our previous findings (10,41) and those of others (29,39). The reduction of osteolysis that we observed in CBZ-treated mice correlates with the findings of the recent phase III clinical trial (METEOR). In the METEOR study, CBZ treatment was associated with reduced skeletal-related events and the decreased levels of osteolytic bone biomarkers in patients with RCCBM (11,12). Thus, CBZ interrupts the cycle of pathologic osteolysis via dual targeting of RCC and RCC-stromal crosstalk. Our studies demonstrate an overlooked and significant aspect of the mechanism that drives pathologic osteolysis.

In conclusion, by using a 3D OSB/Bo-786 co-culture system, we demonstrated that bone-derived 786-O RCC cells exert an inhibitory effect on OSB differentiation, a mechanism that contributes to RCC-mediated osteolysis. RCC-mediated inhibition of OSB differentiation can be reversed using agents that promote OSB differentiation—a novel therapeutic strategy for preventing/treating RCCBM that is refractory to treatment with antiresorptive drugs. The 3D co-culture system provides an *in vitro* model that mimics tumor behavior in the bone microenvironment, and is suitable for screening osteoanabolic agents prior to further testing *in vivo*. The promising preclinical evidence provided in the current study suggests that further testing of the combination therapy strategy of CBZ with osteoanabolic agents in clinical trials for treating RCCBM is warranted.

Supplementary Material

Refer to Web version on PubMed Central for supplementary material.

Acknowledgments

This work was supported by grants from MDACC Institutional Start-up fund, Institutional Research Grant (IRG) Program, and Bridge Funding at the MD Anderson Cancer Center (to R. Satcher), the NIH RO1 CA174798, P50 CA140388, Cancer Prevention and Research Institute of Texas (CPRIT RP110327, RP150179, RP190252) (to S. H. Lin), RP150282 (to G. Gallick), core grant P30 CA016672 (to MDACC), P01CA098912 (to M. Farach-Carson), F31DE025179 (to K. Hubka), NSF IRISE 0966303 and NSF GRFP DGE-1450681 (to M. Martinez)

References

1. Wood SL, Brown JE. Skeletal metastasis in renal cell carcinoma: current and future management options. Cancer Treat Rev 2012;38(4):284–91. [PubMed: 21802857]
2. Woodward E, Jagdev S, McParland L, Clark K, Gregory W, Newsham A, et al. Skeletal complications and survival in renal cancer patients with bone metastases. Bone 2011;48(1):160–6. [PubMed: 20854942]
3. Feng X, McDonald JM. Disorders of bone remodeling. Annu Rev Pathol 2011;6:121–45. [PubMed: 20936937]
4. Zaidi M Skeletal remodeling in health and disease. Nat Med 2007;13(7):791–801. [PubMed: 17618270]
5. Hadjidakis DJ, Androulakis, II. Bone remodeling. Ann N Y Acad Sci 2006;1092:385–96. [PubMed: 17308163]
6. McKay RR, Lin X, Perkins JJ, Heng DY, Simantov R, Choueiri TK. Prognostic significance of bone metastases and bisphosphonate therapy in patients with renal cell carcinoma. Eur Urol 2014;66(3):502–9. [PubMed: 24613250]
7. Pan T, Lin SC, Yu KJ, Yu G, Song JH, Lewis VO, et al. BIGH3 Promotes Osteolytic Lesions in Renal Cell Carcinoma Bone Metastasis by Inhibiting Osteoblast Differentiation. Neoplasia 2018;20(1):32–43. [PubMed: 29190493]

8. Thapa N, Kang KB, Kim IS. Beta ig-h3 mediates osteoblast adhesion and inhibits differentiation. Bone 2005;36(2):232–42. [PubMed: 15780949]

9. Peruzzi B, Cappariello A, Del Fattore A, Rucci N, De Benedetti F, Teti A. c-Src and IL-6 inhibit osteoblast differentiation and integrate IGFBP5 signalling. Nat Commun 2012;3:630. [PubMed: 22252554]

10. Yu KJ, Li JK, Lee YC, Yu G, Lin SC, Pan T, et al. Cabozantinib-induced osteoblast secretome promotes survival and migration of metastatic prostate cancer cells in bone. Oncotarget 2017;8(43):74987–5006. [PubMed: 29088840]

11. Singh H, Brave M, Beaver JA, Cheng J, Tang S, Zahalka E, et al. U.S. Food and Drug Administration Approval: Cabozantinib for the Treatment of Advanced Renal Cell Carcinoma. Clinical cancer research : an official journal of the American Association for Cancer Research 2017;23(2):330–5. [PubMed: 27793960]

12. Choueiri TK, Halabi S, Sanford BL, Hahn O, Michaelson MD, Walsh MK, et al. Cabozantinib Versus Sunitinib As Initial Targeted Therapy for Patients With Metastatic Renal Cell Carcinoma of Poor or Intermediate Risk: The Alliance A031203 CABOSUN Trial. J Clin Oncol 2017;35(6):591–7. [PubMed: 28199818]

13. Lee YC, Cheng CJ, Bilen MA, Lu JF, Satcher RL, Yu-Lee LY, et al. BMP4 promotes prostate tumor growth in bone through osteogenesis. Cancer Res 2011;71(15):5194–203. [PubMed: 21670081]

14. Kale S, Biermann S, Edwards C, Tarnowski C, Morris M, Long MW. Three-dimensional cellular development is essential for ex vivo formation of human bone. Nat Biotechnol 2000;18(9):954–8. [PubMed: 10973215]

15. Tortelli F, Pujic N, Liu Y, Laroche N, Vico L, Cancedda R. Osteoblast and osteoclast differentiation in an in vitro three-dimensional model of bone. Tissue Eng Part A 2009;15(9):2373–83. [PubMed: 19292676]

16. Matthews BG, Naot D, Callon KE, Musson DS, Locklin R, Hulley PA, et al. Enhanced osteoblastogenesis in three-dimensional collagen gels. Bonekey Rep 2014;3:560. [PubMed: 25120910]

17. Hsiong SX, Boontheekul T, Huebsch N, Mooney DJ. Cyclic arginine-glycine-aspartate peptides enhance three-dimensional stem cell osteogenic differentiation. Tissue Eng Part A 2009;15(2):263–72. [PubMed: 18783323]

18. Pan T, Fong EL, Martinez M, Harrington DA, Lin SH, Farach-Carson MC, et al. Three-dimensional (3D) culture of bone-derived human 786-O renal cell carcinoma retains relevant clinical characteristics of bone metastases. Cancer Lett 2015;365(1):89–95. [PubMed: 26004343]

19. Satcher RL, Pan T, Cheng CJ, Lee YC, Lin SC, Yu G, et al. Cadherin-11 in renal cell carcinoma bone metastasis. PLoS One 2014;9(2):e89880. [PubMed: 24587095]

20. Satcher RL, Pan T, Bilen MA, Li X, Lee YC, Ortiz A, et al. Cadherin-11 endocytosis through binding to clathrin promotes cadherin-11-mediated migration in prostate cancer cells. J Cell Sci 2015;128(24):4629–41. [PubMed: 26519476]

21. Lin SC, Lee YC, Yu G, Cheng CJ, Zhou X, Chu K, et al. Endothelial-to-Osteoblast Conversion Generates Osteoblastic Metastasis of Prostate Cancer. Dev Cell 2017;41(5):467–80 e3. [PubMed: 28586644]

22. Lee RJ, Saylor PJ, Michaelson MD, Rothenberg SM, Smas ME, Miyamoto DT, et al. A dose-ranging study of cabozantinib in men with castration-resistant prostate cancer and bone metastases. Clinical cancer research : an official journal of the American Association for Cancer Research 2013;19(11):3088–94. [PubMed: 23553848]

23. Fong EL, Wan X, Yang J, Morgado M, Mikos AG, Harrington DA, et al. A 3D in vitro model of patient-derived prostate cancer xenograft for controlled interrogation of in vivo tumor-stromal interactions. Biomaterials 2016;77:164–72. [PubMed: 26599623]

24. Mosmann T Rapid colorimetric assay for cellular growth and survival: application to proliferation and cytotoxicity assays. J Immunol Methods 1983;65(1–2):55–63. [PubMed: 6606682]

25. Huang WC, Xie Z, Konaka H, Sodek J, Zhau HE, Chung LW. Human osteocalcin and bone sialoprotein mediating osteomimicry of prostate cancer cells: role of cAMP-dependent protein kinase A signaling pathway. Cancer Res 2005;65(6):2303–13. [PubMed: 15781644]

26. Yeung F, Law WK, Yeh CH, Westendorf JJ, Zhang Y, Wang R, et al. Regulation of human osteocalcin promoter in hormone-independent human prostate cancer cells. J Biol Chem 2002;277(4):2468–76. [PubMed: 11684680]
27. Tannir NM, Schwab G, Grunwald V. Cabozantinib: an Active Novel Multikinase Inhibitor in Renal Cell Carcinoma. Curr Oncol Rep 2017;19(2):14. [PubMed: 28247252]
28. Yakes FM, Chen J, Tan J, Yamaguchi K, Shi Y, Yu P, et al. Cabozantinib (XL184), a novel MET and VEGFR2 inhibitor, simultaneously suppresses metastasis, angiogenesis, and tumor growth. Mol Cancer Ther 2011;10(12):2298–308. [PubMed: 21926191]
29. Haider MT, Hunter KD, Robinson SP, Graham TJ, Corey E, Dear TN, et al. Rapid modification of the bone microenvironment following short-term treatment with Cabozantinib in vivo. Bone 2015;81:581–92. [PubMed: 26279137]
30. Lee C, Whang YM, Campbell P, Mulcrone PL, Elefteriou F, Cho SW, et al. Dual targeting c-met and VEGFR2 in osteoblasts suppresses growth and osteolysis of prostate cancer bone metastasis. Cancer Lett 2018;414:205–13. [PubMed: 29174801]
31. Jedeszko C, Paez-Ribes M, Di Desidero T, Man S, Lee CR, Xu P, et al. Postsurgical adjuvant or metastatic renal cell carcinoma therapy models reveal potent antitumor activity of metronomic oral topotecan with pazopanib. Sci Transl Med 2015;7(282):282ra50.
32. Li X, Cao X. BMP signaling and skeletogenesis. Ann N Y Acad Sci 2006;1068:26–40. [PubMed: 16831903]
33. Feng J, Gao J, Li Y, Yang Y, Dang L, Ye Y, et al. BMP4 enhances foam cell formation by BMPR-2/Smad1/5/8 signaling. Int J Mol Sci 2014;15(4):5536–52. [PubMed: 24690996]
34. Mukai S, Yorita K, Kawagoe Y, Katayama Y, Nakahara K, Kamibeppu T, et al. Matriptase and MET are prominently expressed at the site of bone metastasis in renal cell carcinoma: immunohistochemical analysis. Hum Cell 2015;28(1):44–50. [PubMed: 25186085]
35. Basch EM, Scholz M, de Bono JS, Vogelzang N, de Souza P, Marx G, et al. Cabozantinib Versus Mitoxantrone-prednisone in Symptomatic Metastatic Castration-resistant Prostate Cancer: A Randomized Phase 3 Trial with a Primary Pain Endpoint. Eur Urol 2019;75(6):929–37. [PubMed: 30528222]
36. Smith M, De Bono J, Sternberg C, Le Moulec S, Oudard S, De Giorgi U, et al. Phase III Study of Cabozantinib in Previously Treated Metastatic Castration-Resistant Prostate Cancer: COMET-1. J Clin Oncol 2016;34(25):3005–13. [PubMed: 27400947]
37. Vignani F, Bertaglia V, Buttigliero C, Tucci M, Scagliotti GV, Di Maio M. Skeletal metastases and impact of anticancer and bone-targeted agents in patients with castration-resistant prostate cancer. Cancer Treat Rev 2016;44:61–73. [PubMed: 26907461]
38. Escudier B, Powles T, Motzer RJ, Olencki T, Aren Frontera O, Oudard S, et al. Cabozantinib, a New Standard of Care for Patients With Advanced Renal Cell Carcinoma and Bone Metastases? Subgroup Analysis of the METEOR Trial. J Clin Oncol 2018;36(8):765–72. [PubMed: 29309249]
39. Stern PH, Alvares K. Antitumor agent cabozantinib decreases RANKL expression in osteoblastic cells and inhibits osteoclastogenesis and PTHrP-stimulated bone resorption. J Cell Biochem 2014;115(11):2033–8. [PubMed: 25042887]
40. Varkaris A, Corn PG, Parikh NU, Efstathiou E, Song JH, Lee YC, et al. Integrating Murine and Clinical Trials with Cabozantinib to Understand Roles of MET and VEGFR2 as Targets for Growth Inhibition of Prostate Cancer. Clin Cancer Res 2016;22(1):107–21. [PubMed: 26272062]
41. Lee YC, Lin SC, Yu G, Cheng CJ, Liu B, Liu HC, et al. Identification of Bone-Derived Factors Conferring De Novo Therapeutic Resistance in Metastatic Prostate Cancer. Cancer Res 2015;75(22):4949–59. [PubMed: 26530902]

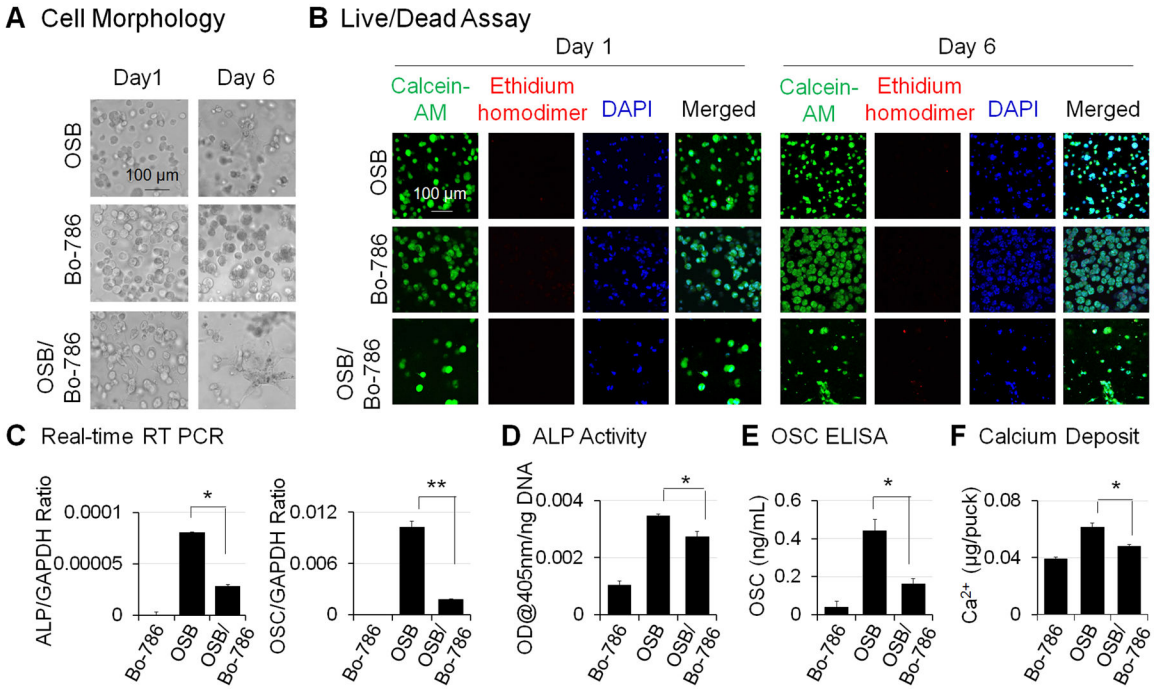

Figure 1. Inhibition of OSB differentiation in 3D co-culture of OSB with Bo-786 cells.

A) Morphology of cells in MC3T3-E1 monoculture (OSB), Bo-786 monoculture (Bo-786), and co-culture of these two cell lines (OSB/Bo-786) in 3D hydrogel on day 1 and day 6. **B)** Cell viability was determined by LIVE/DEAD viability assay. Green staining by calcein-AM indicates viable cells. Red staining by ethidium homodimer indicates non-viable cells. Blue staining by DAPI indicates nucleus. **C)** ALP mRNA and OSC mRNA were determined by real-time RT-PCR; **D)** ALP protein levels were determined by ALP activity assay. **E)** OSC protein levels were determined using OSC ELISA kit. **F)** Calcium assay was used to show calcium deposits in the 3D hydrogel. *: $P < 0.05$; **: $P < 0.01$ as compared to OSB monoculture.

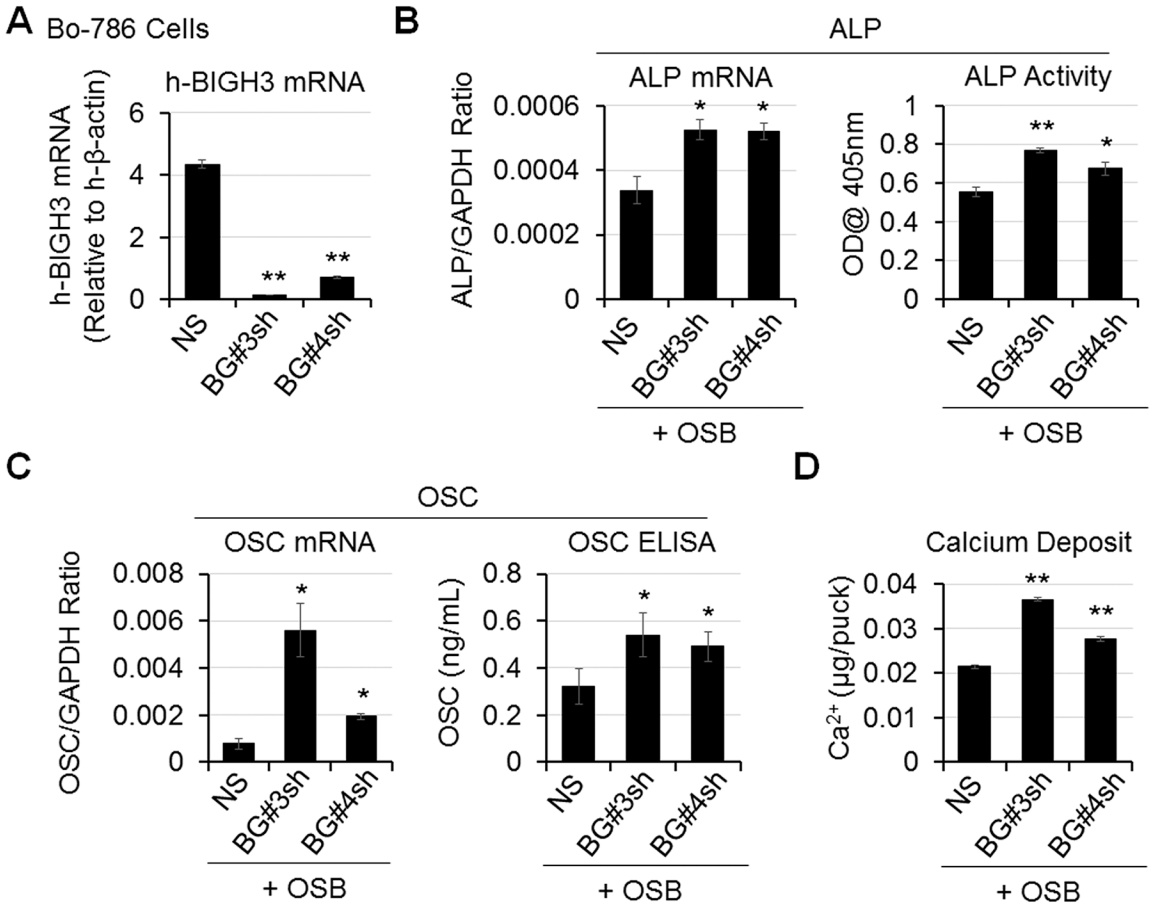

Figure 2. BIGH3 knockdown increased OSB differentiation.

A) BIGH3 mRNA levels in Bo-786 cells with BIGH3 knockdown (Bo-786/BG#3sh and Bo-786/BG#4sh) were confirmed by real-time RT-PCR. **B)** ALP mRNA and protein levels were determined by real-time RT-PCR and by ALP activity assay. **C)** OSC mRNA levels were determined by real-time RT-PCR and OSC protein levels were determined using OSC ELISA kit. **D)** Calcium deposits were determined by calcium assay. *: $P < 0.05$; **: $P < 0.01$ as compared to its control.

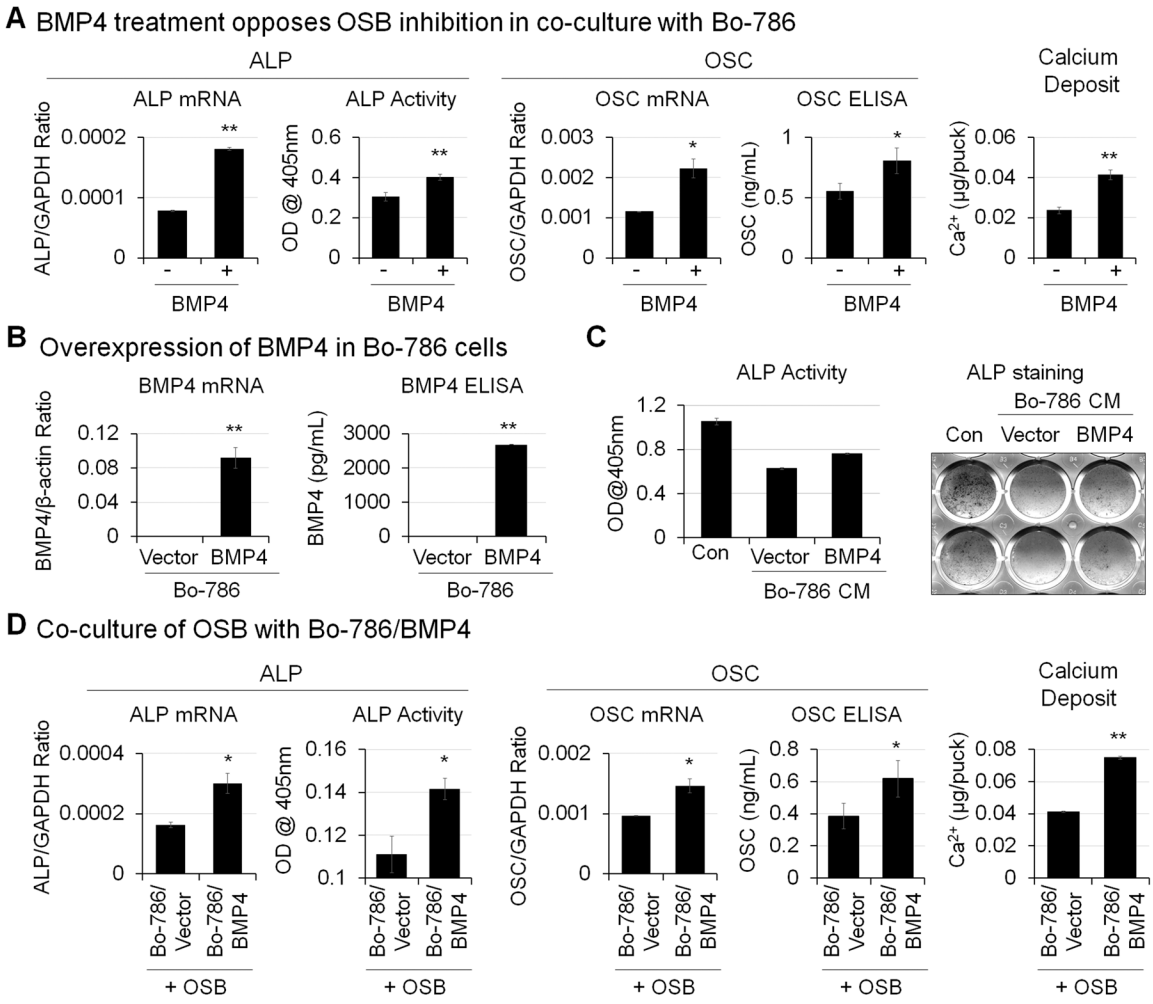

Figure 3. BMP4 enhanced OSB differentiation.

A) OSB were co-cultured with Bo-786 cells in 3D hydrogels and were treated with or without recombinant BMP4 (100 ng/mL). BMP4 was added with each change of medium every other day. ALP mRNA and OSC mRNA were determined by real-time RT-PCR. ALP protein levels were determined by ALP activity assay. OSC protein levels were determined using OSC ELISA kit. Calcium deposits were determined by calcium assay. *: $P < 0.05$; **: $P < 0.01$ as compared to its vehicle control. **B)** BMP4 mRNA in BMP4-overexpressing Bo-786 cells (Bo-786/BMP4) were determined by real-time RT-PCR. The vector-expressing Bo-786 cells (Bo-786/Vector) were used as control. Secreted BMP4 protein levels in cell culture medium were determined using BMP4 ELISA kit. **C)** OSB were cultured in 2D system in ODM and treated with or without conditioned medium from Bo-786/BMP4 or its control Bo-786/vector cells for 14 days followed by ALP staining and ALP activity assay. **D)** OSB were co-cultured with Bo-786/BMP4 cells or with control Bo-786/Vector cells. ALP and OSC mRNA and protein expression and calcium deposits were determined as in (A). *: $P < 0.05$; **: $P < 0.01$ as compared to its vector control.

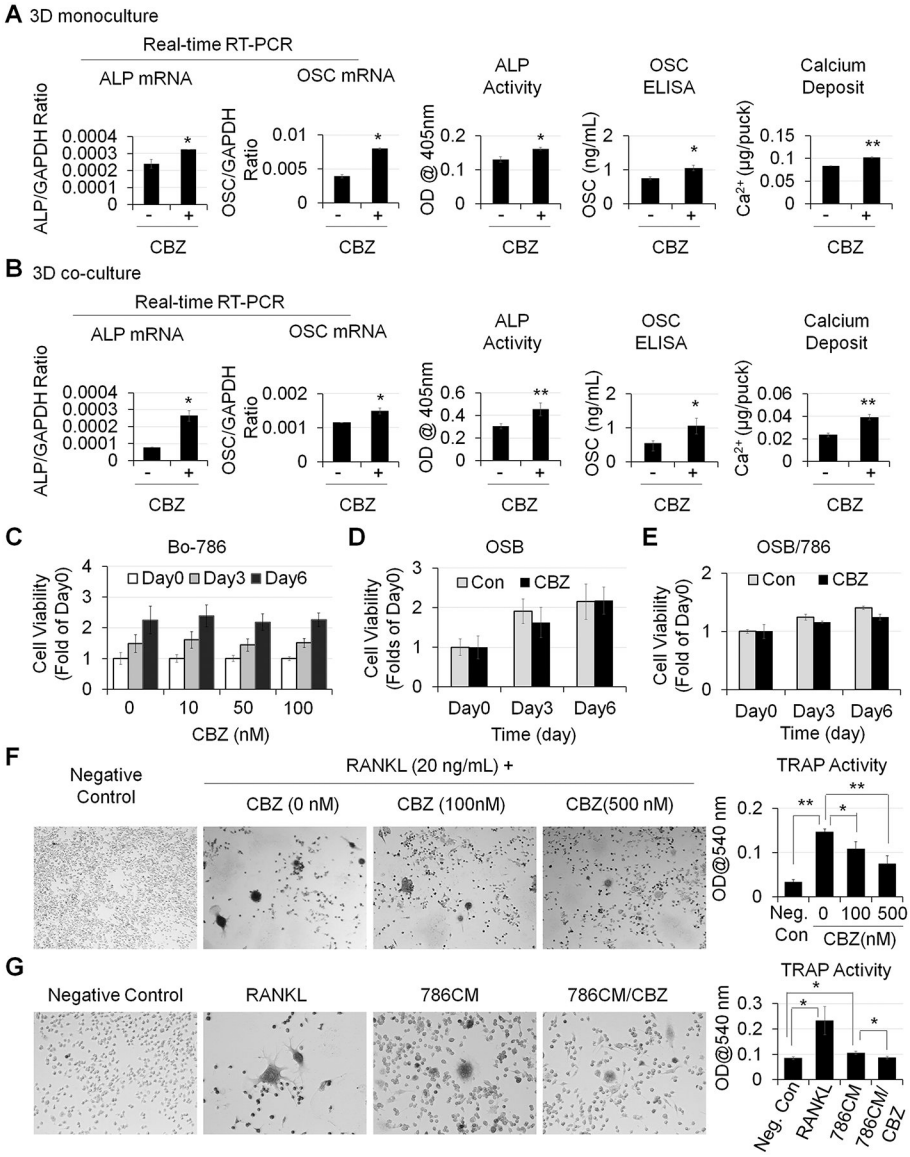

Figure 4. CBZ effects on OSB and osteoclasts *in vitro*.

A) OSB in 3D monoculture and **B)** OSB in 3D co-cultured with Bo-786 cells were treated with or without CBZ (100 nM) in ODM for 6 days. ALP and OSC mRNA and protein levels and calcium deposits were determined as in Fig. 3. **C)** Bo-786 cells cultured in 3D gel were treated with or without CBZ at various concentrations from 0 to 100 nM. Cell viability was determined by PrestoBlue assay. **D)** OSB and **E)** OSB co-cultured with Bo-786 cells in 3D gel were treated with or without CBZ (100 nM). Cell viability was determined by PrestoBlue assay. **F**) RAW264.7 cells were treated with RANKL at 20 ng/mL with or without CBZ (100 nM, 500 nM) for 5 days. Differentiation of RAW264.7 cells was determined by TRAP staining and TRAP activity assay. **G)** RAW264.7 cells were treated with 10-fold concentrated Bo-786 CM with or without CBZ (100 nM) for 5 days. RAW264.7 cells treated with RANKL (50 ng/mL) were used as positive control.

Differentiation of RAW264.7 cells was determined by TRAP staining and TRAP activity assay. *: $P < 0.05$; **: $P < 0.01$.

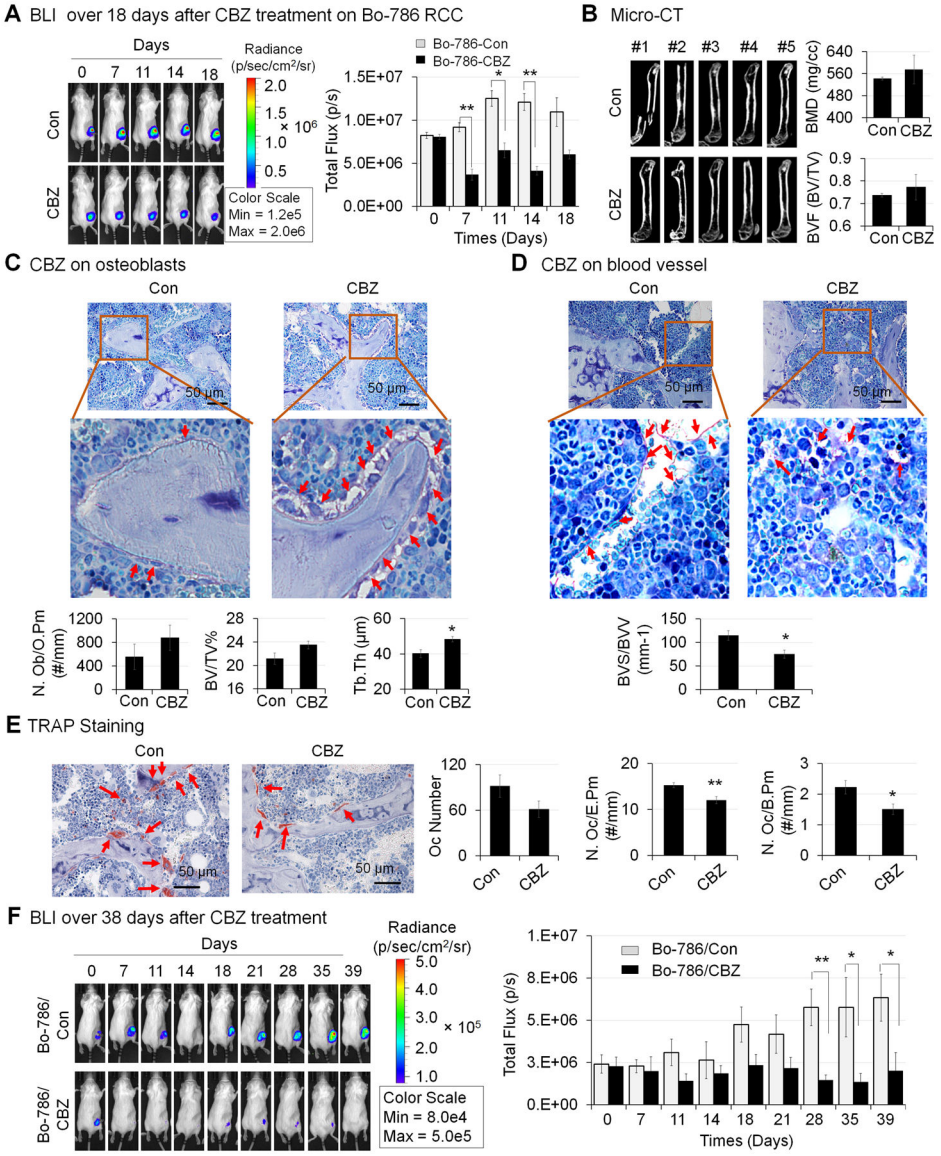

Figure 5. Effects of CBZ on Bo-786 RCC growth in bone and on bone microenvironment *in vivo*.

A) The growth of Bo-786 RCC tumor cells in bone over 18 days after initiation of CBZ treatment was monitored by BLI and total flux values were used for BLI quantification. **B)** Micro-CT analysis of femurs in mice with or without CBZ treatment. Bone mineral density (BMD) and bone volume of whole femur (BVF, BV/TV) was quantified using Microview software. **C)** Bone histomorphometry analysis of number of osteoblasts per osteoid perimeter (N. Ob/O.Pm), bone volume fraction (BV/TV%) (bone volume/Total volume%) and average trabecular thickness (Tb. Th) on Toluidine Blue stained bone sections. **D)** Bone histomorphometry analysis of blood vessel volume (BVV) and blood vessel surface (BVS) on Toluidine Blue stained bone sections. **E)** Bone histomorphometry analysis of number of osteoclasts (Oc Number), number osteoclasts per erosion perimeter (N. Oc/E. Pm), and number of osteoclasts per bone perimeter (N. Oc/B. Pm) on TRAP stained bone sections. **F)** Growth of Bo-786 RCC tumor cells in bone over 39 days after initiation of CBZ treatment

was monitored by BLI and total flux values were used for BLI quantification. *: $P < 0.05$; **: $P < 0.01$ as compared to controls.

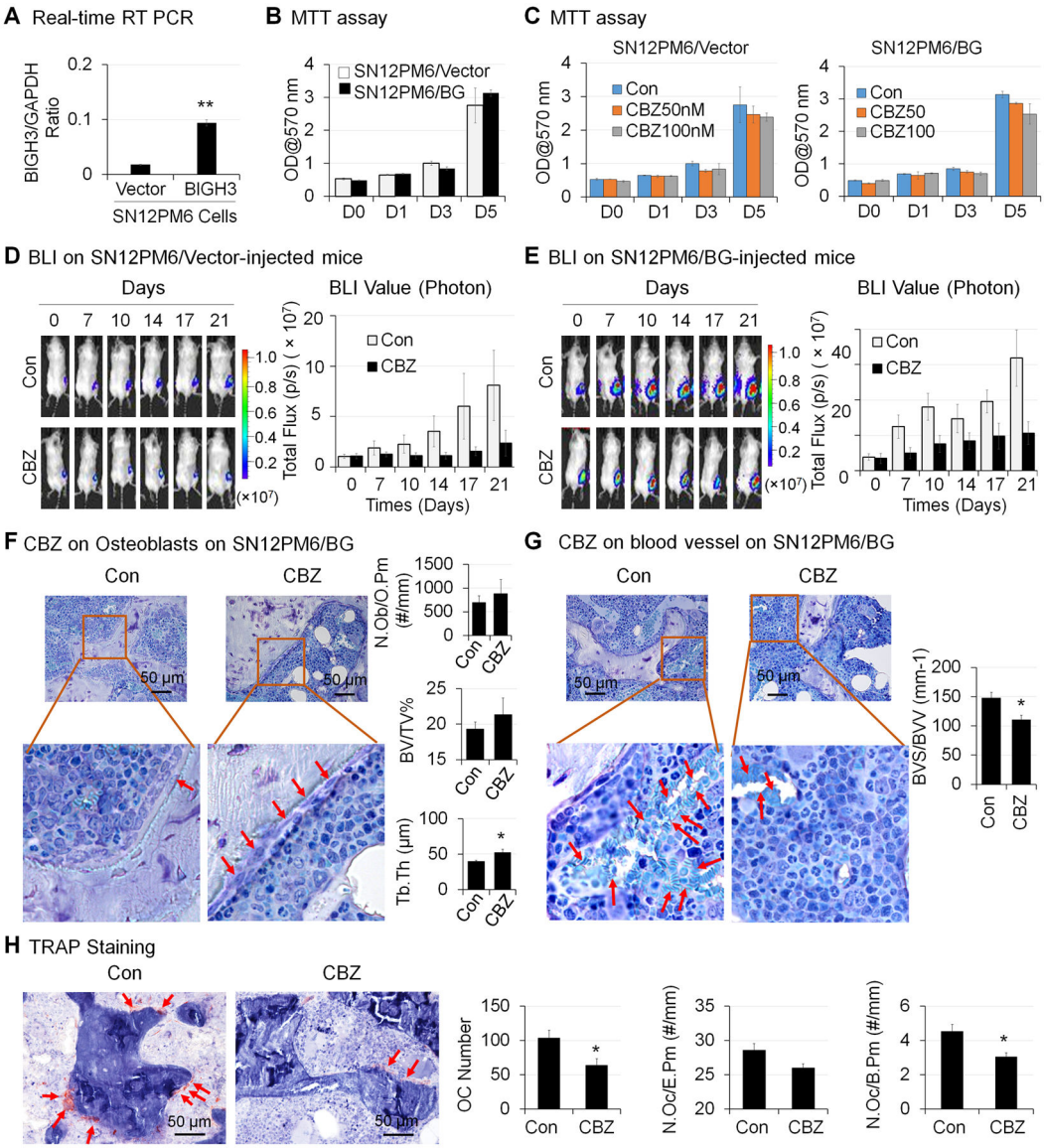

Figure 6. Effects of CBZ on the growth of SN12PM6 RCC in bone *in vivo*.

A) BIGH3 mRNA levels in BIGH3-overexpressing SN12PM6 RCC cells (SN12PM6/BG) and its control SN12PM6/Vector cells were determined by real-time RT-PCR. **B)** Viability of cells in (A) over 5 days were determined by MTT assay. **C)** Cells in (A) were treated with CBZ at 0, 50 nM and 100 nM for 5 days, and cell viability was determined as in (B). The growth of SN12PM6/Vector (**D**) and SN12PM6/BG (**E**) RCC tumor cells in bone over 21 days after initiation of CBZ treatment was monitored by BLI and total flux values were used for BLI quantification. *****: $P < 0.05$; **$P < 0.01$. **F)** Bone histomorphometry analysis of number of osteoblasts per osteoid perimeter (N. Ob/O.Pm), bone volume fraction (BV/TV %) and average trabecular thickness (Tb. Th) on Toluidine Blue stained bone sections. **G)** Bone histomorphometry analysis of blood vessel volume (BVV) and blood vessel surface (BVS) on Toluidine Blue stained bone sections. **H)** Bone histomorphometry analysis of number of osteoclasts (Oc Number), number osteoclasts per erosion perimeter (N. Oc/E.

Pm), and number of osteoclasts per bone perimeter (N. Oc/B. Pm) on TRAP stained bone sections.